Supplementary Information (SI) for Nanoscale.

High-throughput screening of two-dimensional ferromagnetic materials with high Curie temperatures

Shuo Li[a], Chao Jia[a], Haidi Wang[*b], Xingxing Li[*c], and Qunxiang Li[*c]

[a]Key Laboratory of Precision and Intelligent Chemistry, University of Science and Technology of China, Hefei, Anhui 230026, China
[*b]School of Physics, Hefei University of Technology, Hefei, Anhui 230009
[*c]School of Electronic Science and Applied Physics, Hefei University of Technology, Hefei, Anhui 230009

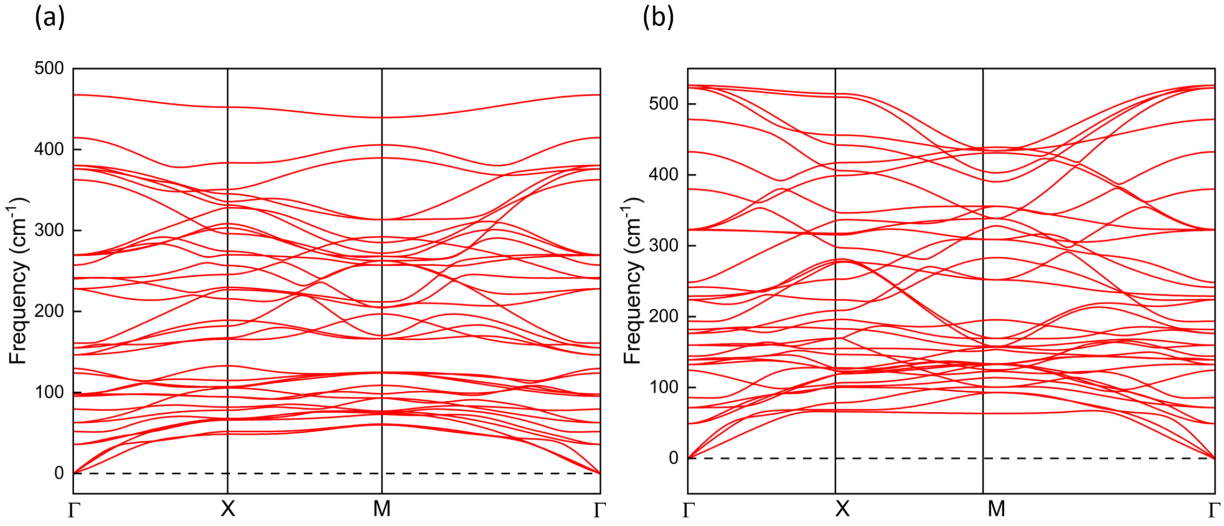

Fig. S1. Phonon spectra of (a) $Ba_3Mn_2I_2O_5$ and (b) $Sr_3Mn_2Cl_2O_5$, calculated with $2 \times 2 \times 1$ supercells.

Further author information:
Haidi Wang: E-mail: haidi@hfut.edu.cn
Xingxing Li: E-mail: lixx@ustc.edu.cn
Qunxiang Li: E-mail: liqun@ustc.edu.cn

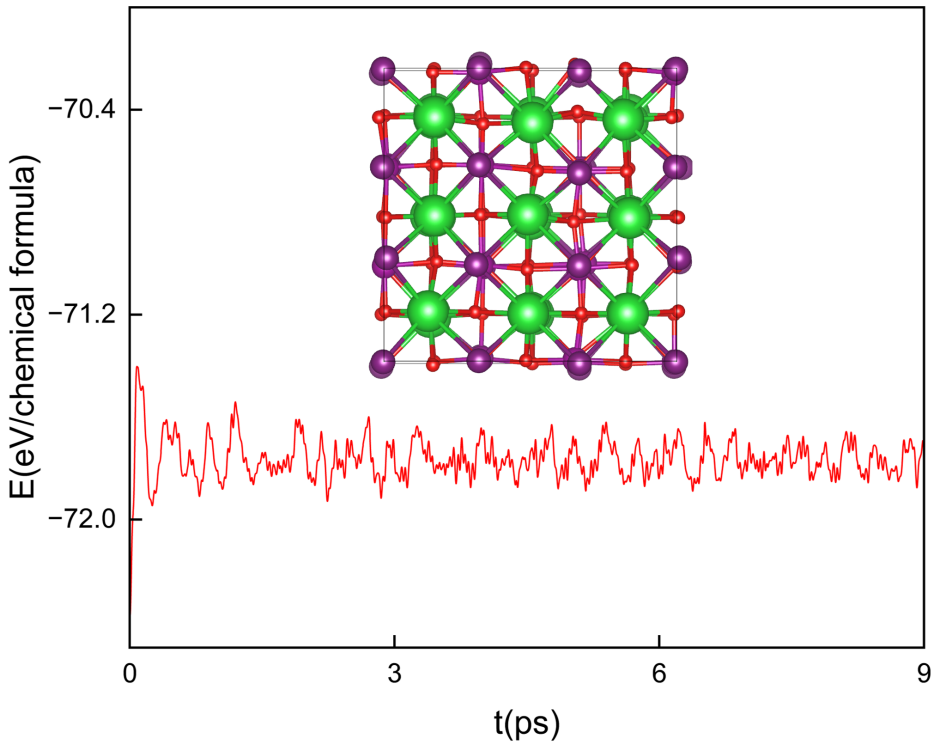

Fig. S2. Total potential energy fluctuation of $Ba_3Mn_2I_2O_5$ nanosheets during ab initio molecular dynamics at 400 K using a $2 \times 2 \times 1$ supercell. The inset shows the snapshot at the end of the simulation.

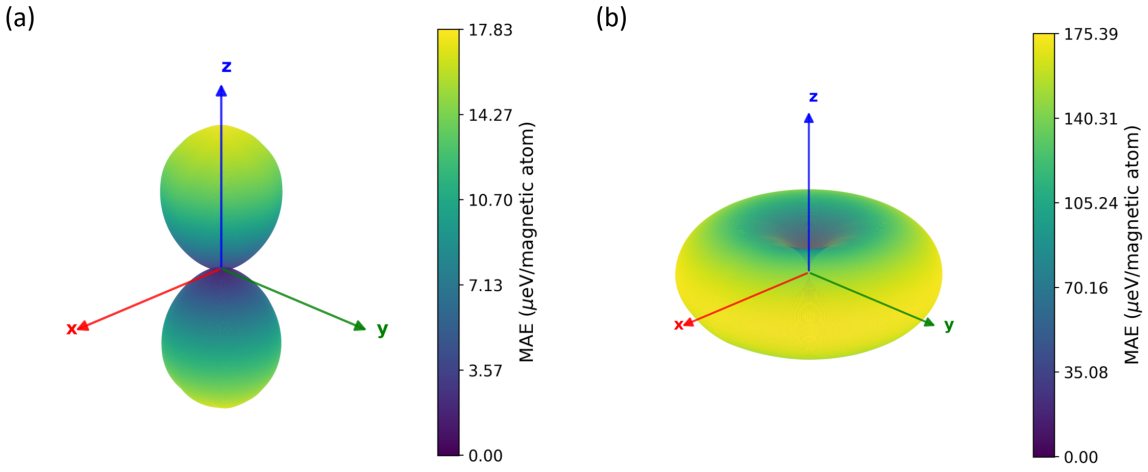

Fig. S3. Magnetocrystalline anisotropy energy (MAE, μeV/magnetic atom) of (a) $Ba_3Mn_2I_2O_5$ and (b) $Sr_3Mn_2Cl_2O_5$.

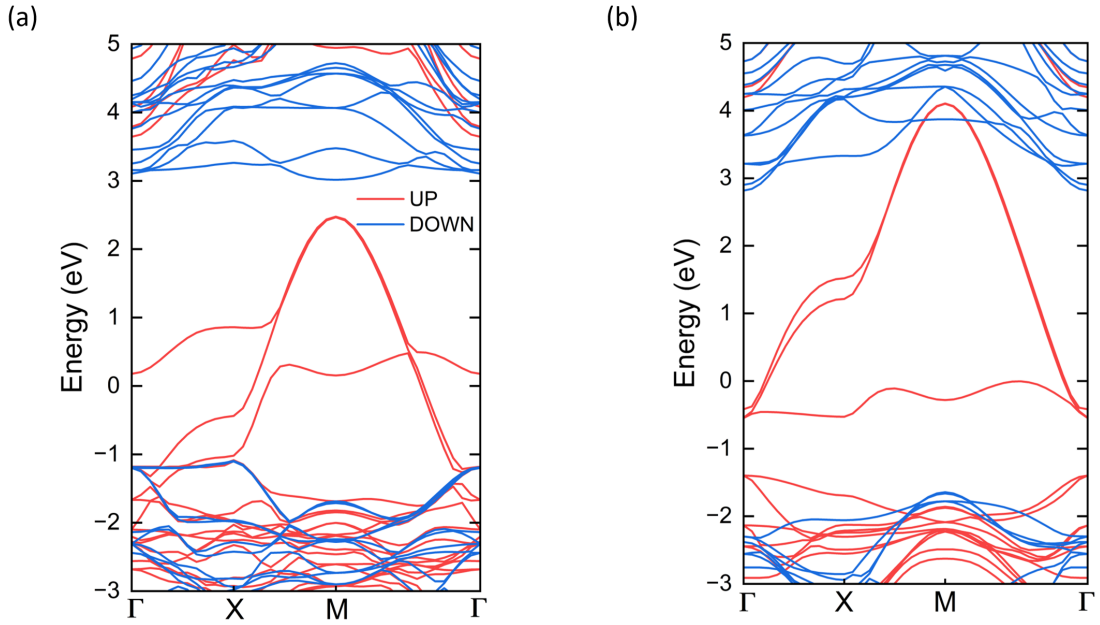

Fig. S4. Band structure of (a) $Ba_3Mn_2I_2O_5$ and (b) $Sr_3Mn_2Cl_2O_5$ based on the HSE06 functional.

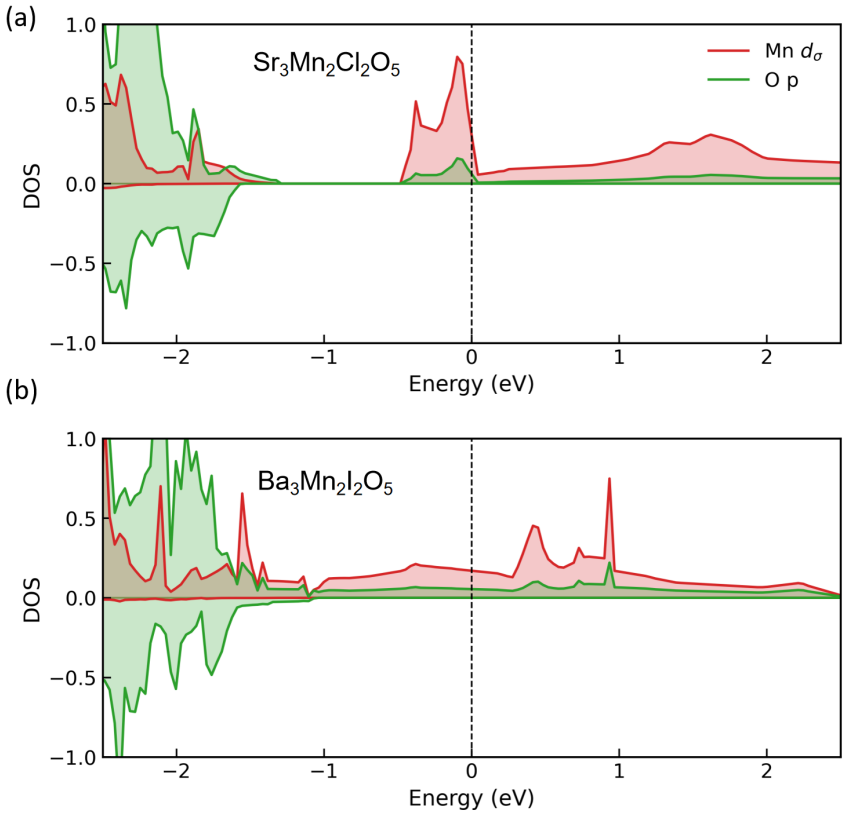

Fig. S5. Density of states of (a) $Sr_3Mn_2Cl_2O_5$ and (b) $Ba_3Mn_2I_2O_5$ calculated using the HSE06 functional.

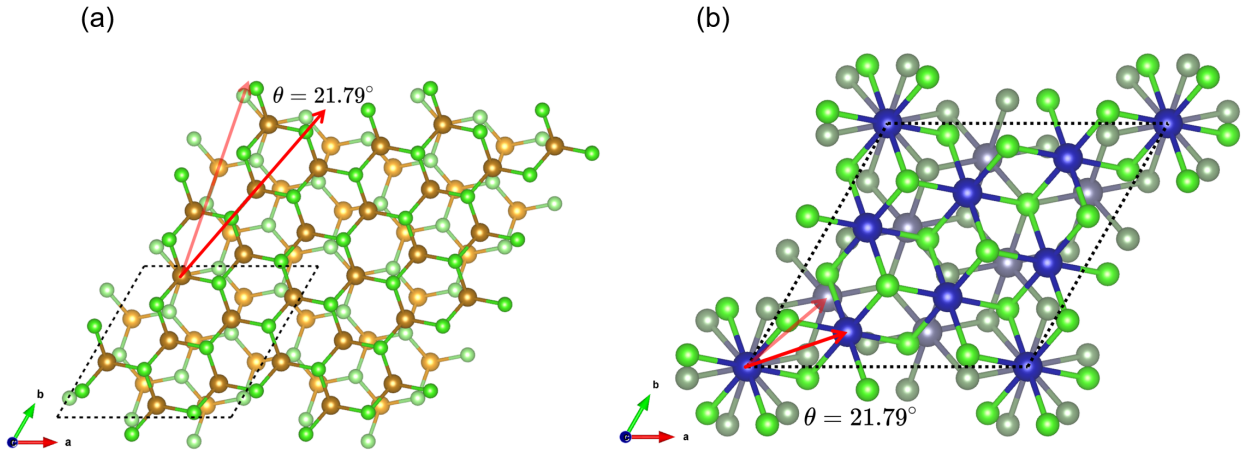

Fig. S6. The crystal structures of bilayer (a) H-$FeCl_2$ and (b) $CoCl_2$, respectively, rotated by $\theta = 21.79°$.

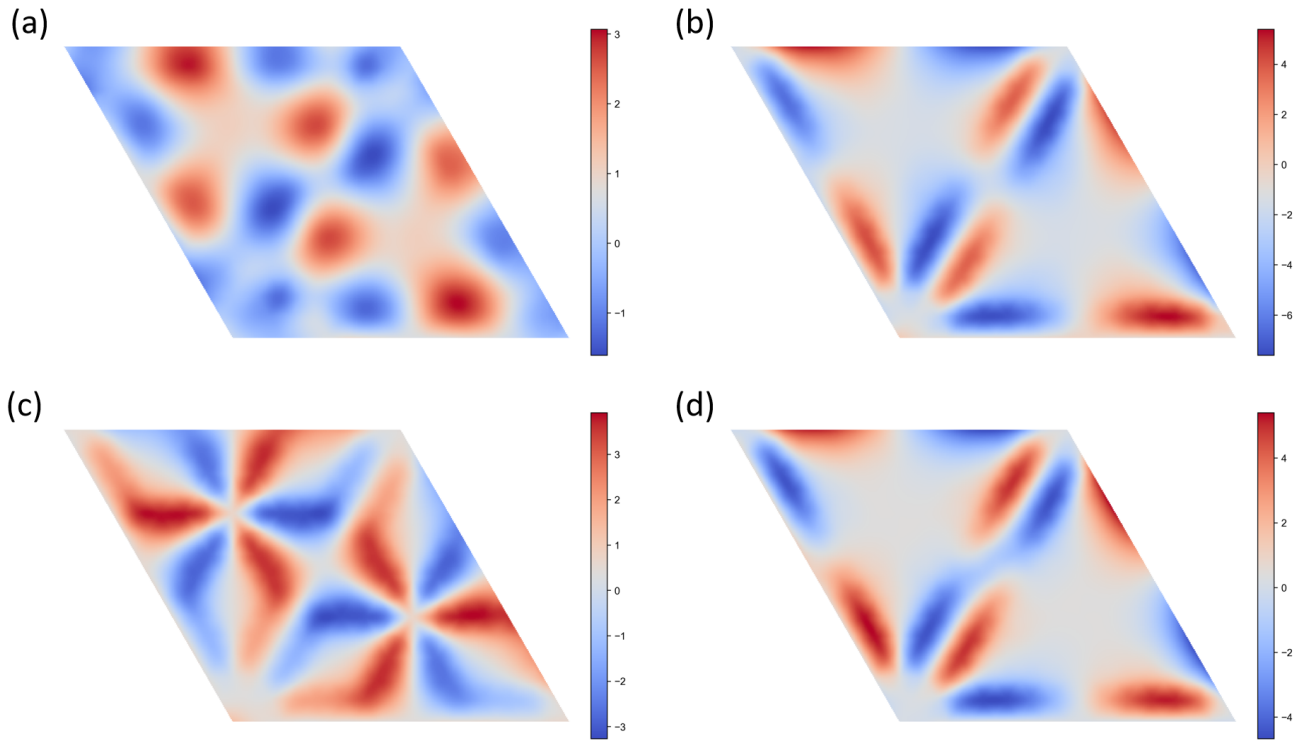

Fig. S7. The spin-splitting energy projections of the (a) HVB and (b) LCB, respectively, for H-$FeCl_2$, while (c) and (d) present the corresponding results for $CoCl_2$. The red (blue) color blocks indicate regions where $E_{\text{spin-up}} > E_{\text{spin-down}}$ ($E_{\text{spin-up}} < E_{\text{spin-down}}$).

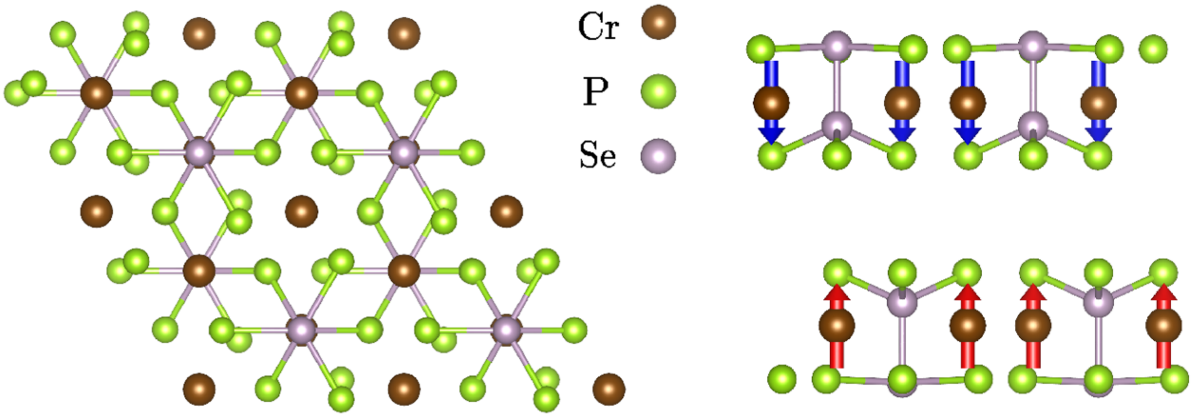

Fig. S8. Bilayer structure of $CrPSe_3$.

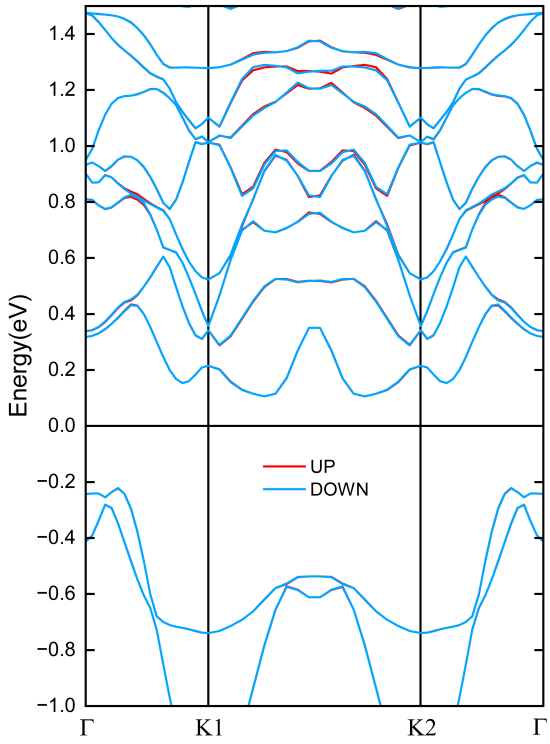

Fig. S9. Band structure of $CrPSe_3$. The path between K1$(\frac{1}{3}, \frac{1}{3})$ and K2$(\frac{1}{3}, -\frac{2}{3})$ is not a high-symmetry path.

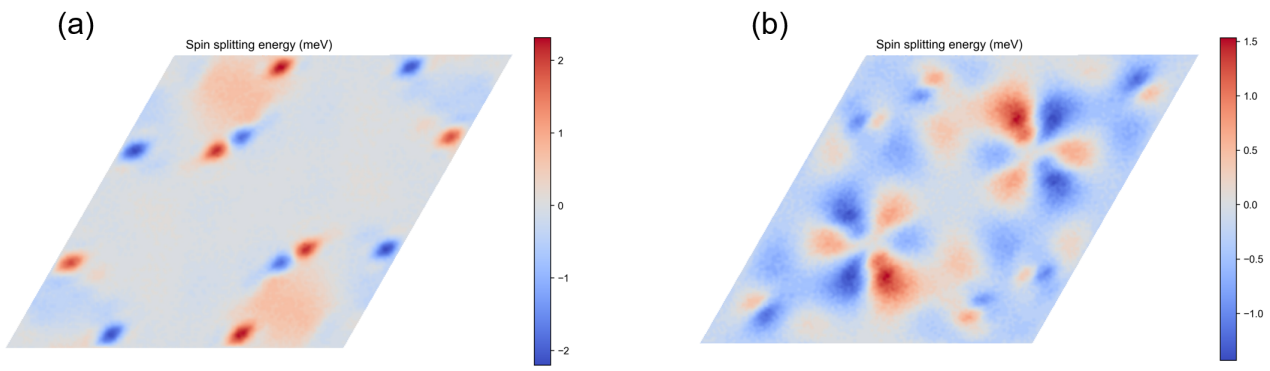

Fig. S10. Spin-splitting energy projections of (a) HVB and (b) LCB, respectively, for $CrPSe_3$, where the red (blue) color block indicates $E_{\mathrm{spin-up}} > E_{\mathrm{spin-down}}$ ($E_{\mathrm{spin-up}} < E_{\mathrm{spin-down}}$).

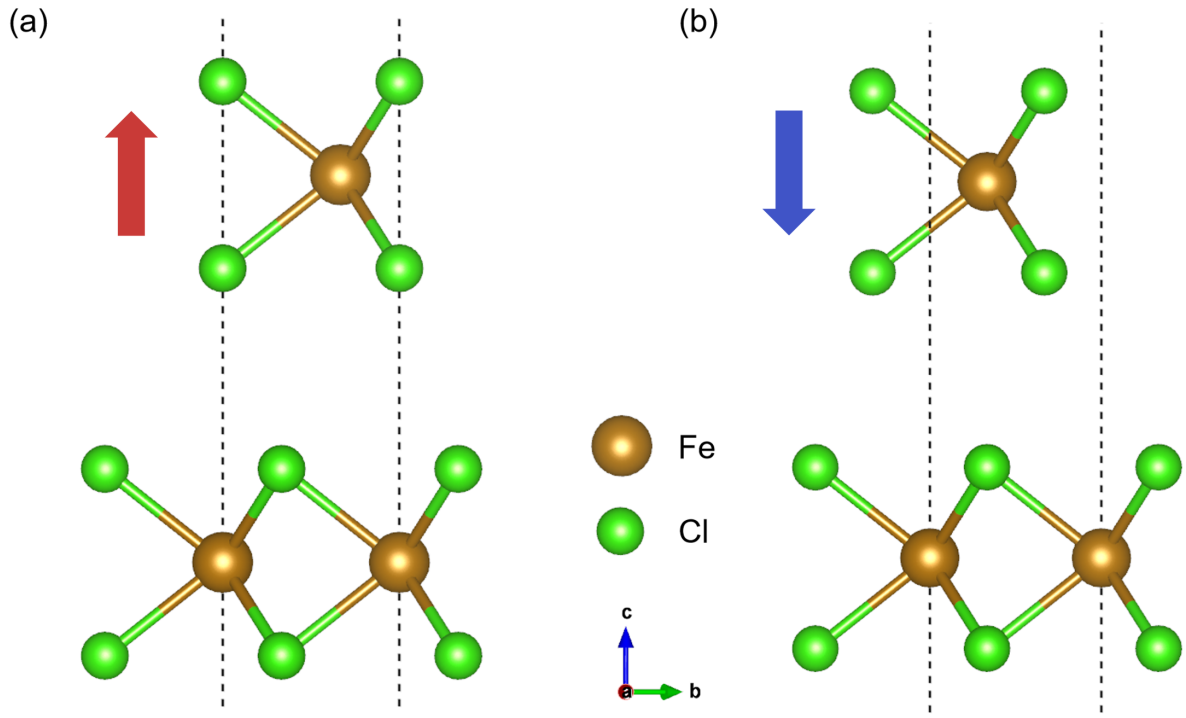

Fig. S11. (a) H-$FeCl_2$'s $(\frac{1}{3}, -\frac{1}{3})$ polarization point. (b) H-$FeCl_2$'s $(\frac{2}{3}, -\frac{2}{3})$ polarization point.

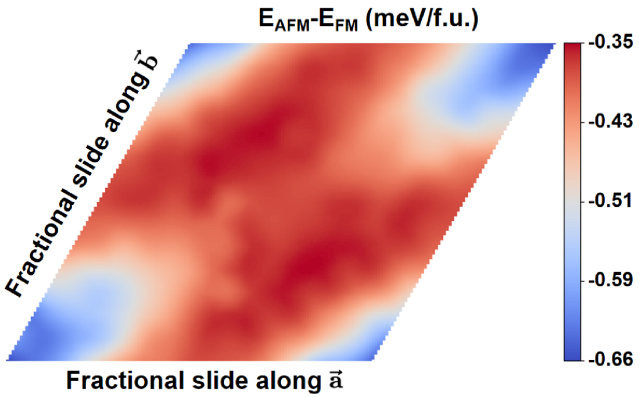

Fig. S12. 2D map of the interlayer exchange energy as a function of fractional lateral slide. The abscissa and ordinate stand for the fractional shift of the H-$FeCl_2$ layer in the $\vec{a}$ and $\vec{b}$ directions of the superlattice, respectively.

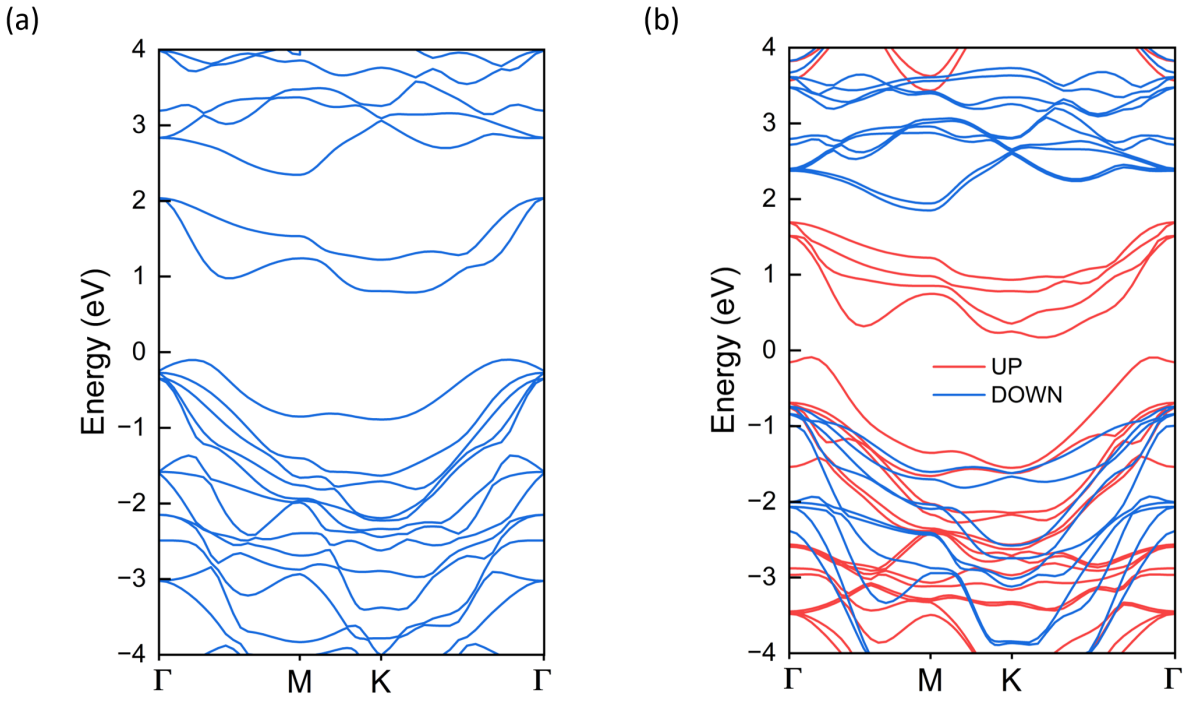

Fig. S13. The band structures of (a) AFM and (b) FM in the ground state of CrSeI during sliding process, respectively.

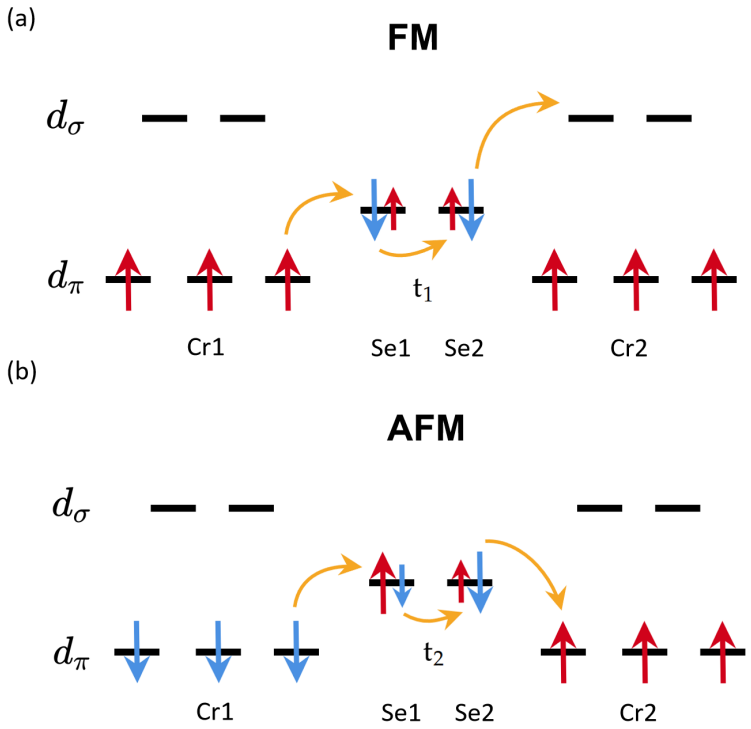

Fig. S14. (a) and (b) Interlayer hopping pathways of T-CeSeI based on super-superexchange interactions for FM and AFM couplings, respectively, where t_1 favors FM order, while t_2 favors AFM order.

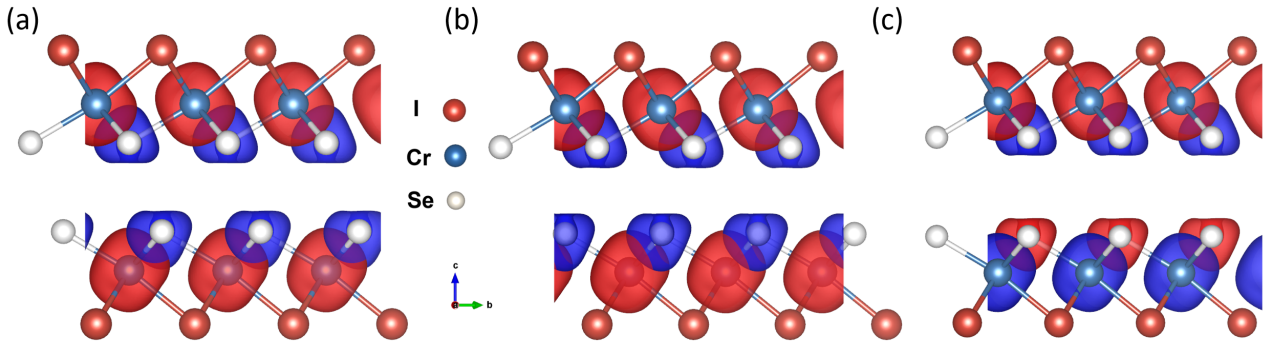

Fig. S15. (a) and (b) are the total spin densities for FM State-I and FM State-II, respectively. (c) is the total spin density for the AFM State-III. We define the bilayer T-CrSeI with interlayer mirror symmetry and an AFM ground state as State-III. The isovalue is set as 0.005 eV/Å^3.

Table. S1. Formula, space group symmetry, exchange interaction constants (J_1, J_2, J_3 in meV), magnetocrystalline anisotropy energy (MAE, μeV/magnetic atom), easy or hard axis direction and lattice constant for the 2D magnetic materials.

	Formula	Symmetry	J_1(meV)	J_2(meV)	J_3(meV)	MAE(μeV/atom)	easy/hard axis	a(Å)	b(Å)
1	$FeCl_2$	P$\bar{6}$m2	54.52	5.33	-5.12	190.42	[001](E)	3.365	3.365
2	Al_2CoSe_4	P$\bar{3}$m1	8.86	3.87	-7.31	35.56	[001](E)	3.773	3.773
3	VBr_3	P$\bar{3}$1m	0.99	16.41	1.37	307.78	[001](H)	6.599	6.599
4	VCl_3	P$\bar{3}$1m	0.004	11.97	-0.0003	291.04	[001](E)	5.960	5.960
5	CrSeI	P3m1	24.16	0.95	-1.06	40.93	[001](H)	3.774	3.775
6	$Ca_3Mn_2I_2O_5$	P4/mmm	11.74	29.84	22.92	47.25	[001](H)	3.942	3.942
7	$CrPSe_3$	P31m	19.52	6.27	-2.23	47.96	[001](H)	6.397	6.398
8	CrSeCl	Pmmn	5.31	15.15	10.92	119.12	[001](H)	5.043	3.536
9	CrSeI	Pmmn	13.53	14.56	14.93	404.24	[100](H)	5.005	3.796
10	$Sr_3Mn_2Cl_2O_5$	P4/mmm	17.03	23.78	12.57	175.39	[001](E)	3.946	3.946
11	CrSCl	Pmmn	4.34	13.86	13.63	28.20	[001](H)	4.755	3.453
12	MnBrO	Pmmn	18.73	32.55	55.01	405.94	[100](E)	3.847	3.431
13	Mn_3CrO_8	P$\bar{3}$m1	14.41	1.86	3.73	90.42	[001](E)	5.840	5.850
14	MnO_2	P$\bar{3}$m1	12.64	0.48	-1.33	325.84	[001](E)	2.894	2.894
15	Mn_2CrO_6	P$\bar{3}$1m	12.46	13.59	-0.47	114.46	[001](H)	5.060	5.060
16	CrSF	Pmmn	4.81	12.64	-1.21	24.64	[001](E)	4.765	3.234
17	MnI_3	P$\bar{3}$1m	14.71	2.24	-1.44	18954.02	[001](H)	7.099	7.099
18	CrSI	Pmmn	12.00	11.36	16.51	573.75	[100](H)	4.723	3.707
19	Sr_2MnClO_3	P4/nmm	3.81	7.18	1.06	444.63	[001](E)	3.899	3.899
20	Sr_2MnIO_3	P4/nmm	6.62	13.25	2.71	343.51	[1-10](H)	3.967	3.967
21	Al_2CoS_4	P$\bar{3}$m1	7.68	4.95	5.46	48.24	[001](E)	3.601	3.601
22	Al_2CoS_4	P$\bar{3}$m1	4.98	1.57	6.81	7.67	[001](E)	3.578	3.578
23	CrTeCl	P3m1	14.26	1.76	-4.71	1351.52	[001](H)	3.700	3.698
24	$CrAsS_3$	P31m	11.98	2.33	1.17	46.56	[001](E)	6.155	6.155
25	$CrHS_2$	P3m1	12.15	0.72	-1.45	4.99	[001](H)	3.573	3.573
26	Ca_2MnIO_3	P4/nmm	2.71	5.41	0.59	240.65	[001](E)	3.873	3.873
27	$CrPS_3$	P31m	11.95	1.15	1.76	54.78	[001](E)	6.064	6.063
28	$CoCl_2$	P$\bar{3}$m1	2.67	1.46	0.96	480.38	[001](H)	3.537	3.537
29	VOF	P$\bar{3}$m1	6.18	3.06	-0.08	79.18	[001](H)	3.310	3.310
30	$CrAuP_2S_6$	P312	5.78	5.77	5.77	135.11	[001](H)	6.055	6.055
31	Sr_2MnClO_3	P4/nmm	3.30	6.59	0.92	419.87	[001](E)	3.899	3.899
32	MnTeI	Pmmn	-3.46	7.15	29.92	6527.09	[001](H)	5.562	3.893
33	$CrAgP_2S_6$	P312	5.19	5.22	5.19	98.93	[001](H)	6.056	6.056
34	CrOF	Pmmn	4.13	3.37	7.59	136.60	[100](H)	3.009	3.911
	$Ba_3Mn_2I_2O_5$	P4/mmm	131.40	43.05	8.07	17.83	[001](H)	4.160	4.160

Table. S2. Magnetic parameters calculated in relevant literature: Formula, Software used for calculation, exchange energy per magnetic atom (E_{ex}, meV), exchange interaction constants (J_1, J_2, J_3 in meV), magnetocrystalline anisotropy energy (MAE, μeV/magnetic atom), easy or hard axis direction, Curie temperature, reference.

	Formula	software	E_{ex}(meV)	J_1(meV)	J_2(meV)	J_3(meV)	MAE(μeV/atom)	easy/hard axis	T_c	Ref
1	$FeCl_2$	VASP	214.73	54.52	5.33	-5.12	190.42	[001](E)	701	this work
1	$FeCl_2$	GPAW	242.24	-	-	-	-	-	202	[1]
1	$FeCl_2$	VASP	250	-	-	-	420	-	-	[2]
1	$FeCl_2$	QE	123.44	3.86	-	-	460	[001](E)	-	[3]
3	VBr_3	VASP	126.73	0.99	16.41	1.37	307.78	[001](H)	253	this work
3	VBr_3	WIEN2k	-	5.2	-	-	1900	[001](H)	20	[4]
4	VCl_3	VASP	108.01	0.004	11.97	-0.0003	291.04	[001](E)	157	this work
4	VCl_3	GPAW	-	-	-	-	-	-	134	[5]
5	CrSeI	VASP	95.49	24.16	0.95	-1.06	40.93	[001](H)	296	this work
5	CrSeI	VASP	-	26.24	0.82	-2.04	-	-	334	[6]
5	CrSeI	VASP	-	25.40	0.81	-3.15	-	-	-	[7]
8	CrSeCl	VASP	61.99	5.31	15.15	10.92	119.12	[001](H)	204	this work
8	CrSeCl	GPAW	-	7.05	5.81	-	38	[001](H)	130	[1]
8	CrSeCl	VASP	-	12.3	13.6	-4.6	179	[100](E)	110	[8]
8	CrSeCl	VASP	-	5.94	15.3	2.52	10	[010](E)	118	[9]
9	CrSeI	VASP	60.47	13.53	14.56	14.93	404.24	[100](H)	257	this work
9	CrSeI	VASP	-	13.6	16.4	1.4	921	[001](E)	192	[8]
9	CrSeI	VASP	-	14.04	16.515	5.31	20	[010](E)	164	[9]
11	CrSCl	VASP	56.59	4.34	13.86	13.63	28.20	[001](H)	208	this work
11	CrSCl	GPAW	-	6.52	3.99	-	26	[001](H)	130	[1]
11	CrSCl	VASP	-	11.7	13.6	3.6	7	[010](H)	161	[8]
11	CrSCl	VASP	-	4.05	13.41	5.67	20	[001](H)	108	[9]
11	CrSCl	VASP	62	14.895	30.87	-	56	[010](H)	150	[10]
14	MnO_2	VASP	51.97	12.64	0.48	-1.33	325.84	[001](E)	127	this work
14	MnO_2	GPAW	30.15	-	-	-	-	-	63	[1]
14	MnO_2	GPAW	-	-	-	-	-	-	17	[5]
14	MnO_2	VASP	62	13.76	-	-	-	-	140	[11]
17	MnI_3	VASP	50.00	14.71	2.24	-1.44	18954.02	[001](H)	166	this work
17	MnI_3	VASP	-	-	-	-	8681.4	[001](H)	253	[12]
18	CrSI	VASP	49.04	12.00	11.36	16.51	573.75	[100](H)	244	this work
18	CrSI	GPAW	-	5.71	4.85	-	223	[100](H)	140	[1]
18	CrSI	VASP	-	13.5	12.9	7.2	1022	[010](H)	203	[8]
18	CrSI	VASP	-	13.815	11.205	7.605	60	[010](E)	146	[9]
18	CrSI	VASP	68	34.155	15.255	-	913	[010](H)	170	[10]
28	$CoCl_2$	VASP	33.06	2.67	1.46	0.96	480.38	[001](H)	86	this work
28	$CoCl_2$	GPAW	412.29	-	-	-	-	-	55	[1]
28	$CoCl_2$	GPAW	-	-	-	-	-	-	25	[5]
28	$CoCl_2$	QE	53.05	-	-	-	-	-	85	[13]
34	CrOF	VASP	14.54	4.13	3.37	7.59	136.60	[100](H)	82	this work
34	CrOF	VASP	-	4.0	3.6	7.7	32	[001](E)	82	[8]
34	CrOF	VASP	-	2.86	4.92	9.04	-	-	150	[14]

Note: In Table S2, we compare our calculated results with those reported in previous studies. Some discrepancies are observed, which mainly arise from the insufficient accuracy in describing exchange interactions. If the Curie temperature is estimated only from the total exchange energy or by considering solely the nearest-neighbor exchange interaction J_1, the calculated values may exhibit significant deviations. As shown in our results, the next-nearest-neighbor J_2 and third-nearest-neighbor J_3 interactions also play non-negligible roles in determining the magnetic properties of the system and therefore must be taken into account for a more reliable estimation of the Curie temperature. The significant discrepancy between our calculated Curie temperature of VBr_3 and those reported in other works can be attributed to the completeness of the spin Hamiltonian (e.g., whether long-range exchange interactions are included) and the differences in the adopted lattice parameters.

Table. S3. Material type classified based on the density of states calculated with the HSE06 functional for the 34 two-dimensional magnetic materials: the spin-flip gap in conduction band (Δ_1, eV), the spin-flip gap in valence band (Δ_2, eV), total band gap(Δ_3, eV), spin up band gap(Δ_4, eV), spin down band gap(Δ_5, eV).

	Formula	Type	Δ_1(eV)	Δ_2(eV)	Δ_3(eV)	Δ_4(eV)	Δ_5(eV)
1	$FeCl_2$	HSC	2.17	0.92	2.57	5.66	2.57
2	Al_2CoSe_4	BMS	0.11	0.66	1.46	1.57	2.13
3	VBr_3	HSC	1.21	0.61	2.03	2.03	3.85
4	VCl_3	HSC	1.06	0.98	2.43	2.43	4.47
5	CrSeI	HSC	1.34	0.13	1.74	1.74	3.21
6	$Ca_3Mn_2I_2O_5$	HMF	-	-	-	-	3.77
7	$CrPSe_3$	HSC	0.33	0.03	0.67	0.67	1.03
8	CrSeCl	BMS	1.86	0.13	0.87	0.99	2.73
9	CrSeI	HSC	1.85	0.16	0.79	0.79	2.80
10	$Sr_3Mn_2Cl_2O_5$	HMF	-	-	-	-	4.38
11	CrSCl	HSC	1.36	0.19	1.90	1.90	3.45
12	MnBrO	HMF	-	-	-	-	4.01
13	Mn_3CrO_8	HSC	1.50	0.44	1.94	1.94	3.88
14	MnO_2	HMF	-	-	-	-	4.18
15	Mn_2CrO_6	HSC	1.44	0.54	1.91	1.91	3.89
16	CrSF	BMS	1.79	0.42	1.35	1.76	3.14
17	MnI_3	HSC	3.12	0.65	0.10	0.10	3.87
18	CrSI	HSC	1.45	0.19	1.42	1.42	3.06
19	Sr_2MnClO_3	HSC	2.68	0.91	0.59	0.59	4.18
20	Sr_2MnIO_3	HMF	-	-	-	-	3.46
21	Al_2CoS_4	BMS	0.31	0.88	1.90	2.21	2.78
22	Al_2CoS_4	BMS	0.04	0.87	1.90	1.94	2.77
23	CrTeCl	BMS	1.34	1.16	1.01	2.17	2.39
24	$CrAsS_3$	BMS	0.03	0.12	1.51	1.54	1.63
25	$CrHS_2$	HSC	0.25	0.09	2.82	2.82	3.17
26	Ca_2MnIO_3	HSC	2.51	0.00	0.55	0.55	3.06
27	$CrPS_3$	HSC	0.56	0.03	1.13	1.13	1.72
28	$CoCl_2$	BMS	2.41	0.33	4.15	6.57	4.48
29	VOF	HMF	-	-	-	-	6.32
30	$CrAuP_2S_6$	HSC	1.12	0.00	1.51	1.51	2.63
31	Sr_2MnClO_3	HSC	2.62	0.87	0.66	0.66	4.16
32	MnTeI	HMF	-	-	-	-	1.91
33	$CrAgP_2S_6$	HSC	1.10	0.06	1.94	1.94	3.10
34	CrOF	HSC	1.13	1.50	3.86	3.86	6.48

REFERENCES

[1] Torelli, D., Thygesen, K. S., and Olsen, T., "High throughput computational screening for 2D ferromagnetic materials: the critical role of anisotropy and local correlations," *2D Mater.* **6**(4), 045018 (2019).

[2] Zheng, H., Han, H., Zheng, J., and Yan, Y., "Strain tuned magnetocrystalline anisotropy in ferromagnetic H-$FeCl_2$ monolayer," *Solid State Commun.* **271**, 66 (2018).

[3] Yang, X., Shen, Y., Lv, L., Zhou, M., Zhang, Y., Meng, X., Jiang, X., Ai, Q., Shuai, Y., and Zhou, Z., "Tuning the topological phase and anomalous hall conductivity with magnetization direction in H-$FeCl_2$ monolayer," *Appl. Phys. Lett.* **123**(20), 203102 (2023).

[4] Liu, L., Yang, K., Wang, G., and Wu, H., "Two-dimensional ferromagnetic semiconductor VBr_3 with tunable anisotropy," *J. Mater. Chem. C* **8**(42), 14782 (2020).

[5] Torelli, D., Moustafa, H., Jacobsen, K. W., and Olsen, T., "High-throughput computational screening for two-dimensional magnetic materials based on experimental databases of three-dimensional compounds," *npj Comput. Mater.* **6**(1), 158 (2020).

[6] Zhu, H.-R., Shao, B., and Zuo, X., "Enhancing ferromagnetic coupling in CrXY (X= O, S, Se; Y= Cl, Br, I) monolayers by turning the covalent character of Cr-X bonds," *npj Comput. Mater.* **9**(1), 56 (2023).

[7] Li, P., Yu, D., Liang, J., Ga, Y., and Yang, H., "Topological spin textures in 1T-phase janus magnets: Interplay between dzyaloshinskii-moriya interaction, magnetic frustration, and isotropic higher-order interactions," *Phys. Rev. B* **107**(5), 054408 (2023).

[8] He, W., Yin, Y., Gong, Q., Evans, R. F., Gutfleisch, O., Xu, B.-X., Yi, M., and Guo, W., "Giant magnetocaloric effect in magnets down to the monolayer limit," *Small* **19**(36), 2300333 (2023).

[9] Wang, C., Zhou, X., Zhou, L., Tong, N.-H., Lu, Z.-Y., and Ji, W., "A family of high-temperature ferromagnetic monolayers with locked spin-dichroism-mobility anisotropy: MnNX and CrCX (X= Cl, Br, I; C= S, Se, Te)," *Sci. Bull.* **64**(5), 293 (2019).

[10] Guo, Y., Zhang, Y., Yuan, S., Wang, B., and Wang, J., "Chromium sulfide halide monolayers: intrinsic ferromagnetic semiconductors with large spin polarization and high carrier mobility," *Nanoscale* **10**(37), 18036 (2018).

[11] Kan, M., Zhou, J., Sun, Q., Kawazoe, Y., and Jena, P., "The intrinsic ferromagnetism in a MnO_2 monolayer," *J. Phys. Chem. Lett.* **4**(20), 3382 (2013).

[12] Li, Y., Fu, H., Qi, Q., Li, Z., Ma, Y., Wu, X., and Zhong, C., "Interatomic doping regulating the electronic structure and magnetic anisotropy of MnI_3 monolayer: A first-principles study," *J. Appl. Phys.* **137**(21), 214302 (2025).

[13] Kulish, V. V. and Huang, W., "Single-layer metal halides MX_2 (X= Cl, Br, I): stability and tunable magnetism from first principles and monte carlo simulations," *J. Mater. Chem. C* **5**(34), 8734 (2017).

[14] Xiao, T., Wang, G., and Liao, Y., "Theoretical prediction of two-dimensional crof sheet as a ferromagnetic semiconductor or a half-metal," *Chem. Phys.* **513**, 182 (2018).